



**A targetable acid-reponsive micellar system for signal activation based high performance surgical resolution of tumors**

Journal:	<i>Biomaterials Science</i>
Manuscript ID:	BM-ART-01-2014-000007.R1
Article Type:	Paper
Date Submitted by the Author:	21-Jan-2014
Complete List of Authors:	Han, Shoufa; Xiamen University, Chemcial Biology Wu, Xuanjun; Xiamen University, Chemistry Tian, Yunpeng; Xiamen University, Chemical biology Yu, Mingzhu; Xiamen University, Chemical biology Han, Jiahuai; Xiamen University,

Cite this: DOI: 10.1039/c0xx00000x

www.rsc.org/xxxxxx

ARTICLE TYPE

# A targetable acid-reponsive micellar system for signal activation based high performance surgical resolution of tumors

Xuanjun Wu,<sup>a</sup> Yunpeng Tian,<sup>a</sup> Mingzhu Yu,<sup>a</sup> Jiahuai Han,<sup>b</sup> and Shoufa Han<sup>a,\*</sup>

Received (in XXX, XXX) Xth XXXXXXXXX 20XX, Accepted Xth XXXXXXXXX 20XX

DOI: 10.1039/b000000x

Tumor-reporting probes are valuable to guide surgical resection of tumor foci evasive to visual inspection. As tumors display distinct arrays of lectins, we herein report the construction and screening of a panel of glycan-displaying smart micelles for tumor illumination in mice. These micelles consist of cores of rhodamine-sultam (RST) responsive to lysosomal acidity and corona of poly[(styrene-*alter*-(maleic acid))] glycosylated with D-glucosamine, D-mannosamine or D-galactosamine. These nanoscale micelles are nonfluorescent extracellularly and become luminescent within acidic lysosomes, enabling optical tracking of tumor endocytosis of the micelles. *In vivo* screening revealed high-efficiency uptake and fluorescence activation of galactosylated micelles (RST@P-Gal) by subcutaneous tumor and disseminated liver tumor foci with diameters of 0.1-10 mm, which is significantly below minimal residual cancer (a minimum of 1-cm clearance). This system is readily adapted to illuminate different tumors by expanding the diversity of glycans on the shell. Given the robustness and high performance of this system, lectin-targeted responsive micelles are attractive for diagnosis or surgical ablation of tumors.

## Introduction

With the global prevalence of cancer, methods that could improve the outcome of available modalities for cancer treatment are of clinical significance. Surgical resection is widely used in treatment of tumors where the limited visibility of tumor foci under visual inspection often results in incomplete removal and hence tumor relapse. As such luminescent probes that could direct surgeons to evasive tumor foci are of significant values.<sup>[1]</sup> The utility of fluorescence guided oncogenic surgery has been demonstrated by a number of clinical demonstrations, *e.g.* imaging of epithelial ovarian cancer with fluorescein-isothiocyanate tagged folate.<sup>[2]</sup> Conventional dyes lack the ability to recognize tumors and thus are often integrated with tumor-targetable biochemical entities such as monoclonal antibody, folate, and fluorogenic substrates specific for tumoral enzymes, etc.<sup>[2-3]</sup> Apart from selectivity, optical systems that could be activated to the fluorescence-on states inside tumors while being nonfluorescent in off-target settings are advantageous owing to the intrinsic low-background signals and improved discern of tumors.<sup>[4]</sup> In this regard, optical probes responsive to lysosomal pH of tumors are attractive for imaging viable cancer cells.<sup>[3c, 4g]</sup>

Cell surface protein-glycan interactions mediated a wealth of biological events ranging from cell trafficking, endocytosis to cancer metastasis, etc.<sup>[5]</sup> Glycan-binding proteins, known as lectins, are often expressed in patterns unique to defined cell lines or tissues, and thus are attractive targets for glycan mediated delivery of therapeutics.<sup>[6]</sup> To date, the use of glyco-probes with responsive properties has been largely unexplored for surgical tumor detection. To develop targetable systems for intraoperative tumor imaging, we report the construction and screening of a group of carbohydrate-displaying polymeric micelles with lysosome-activatable fluorescence in subcutaneous tumor and liver tumor models. The probes consist of hydrophilic shells of glycosylated poly[(styrene-*alter*-(maleic acid))] and hydrophobic cores of rhodamine-sultam (RST) which isomerizes into highly

fluorescent species upon internalization into lysosomes (Fig. 1). Studies in tumor-bearing mice reveal that lectin-targeted glyco-micelles possess features advantageous for low-background detection of disseminated tumor foci during oncogenic surgery.

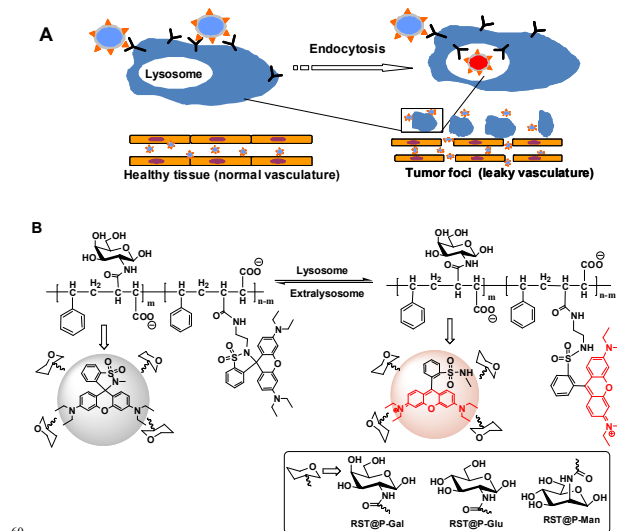


**Fig. 1** Tumor imaging with lectin-targeted acid responsive micelles. (A) Illustration of tumor illumination with glyco-micelles by virtue of enhanced permeability and retention (EPR) effects of tumor vasculature, tumor surface lectin mediated endocytosis, and signal activation of internalized micelles within lysosomes. (B) proton mediated fluorescence activation of RST moieties of the micellar system.

## Results and Discussion

Endocytic lectins are often expressed on in a tissue- or cell type-dependent manner.<sup>[7]</sup> For instance, mannose receptors are rich in macrophages<sup>[8]</sup> whereas asialoglycoprotein receptors

(ASGPR) that bind terminal galactose on proteins are abundantly expressed on the plasma membrane of hepatocytes.<sup>[9]</sup> Much effort has been devoted to the use of glycan-bearing vectors for delivery of therapeutics by targeting cell surface lectins such as ASPGR,<sup>[10]</sup> mannose receptors,<sup>[11]</sup> and Siglecs, etc.<sup>[12]</sup> In contrast, there is a lack on the use of glyco-probes for fluorescence-guided tumor detection. As mentioned above, optical probes that are emissive in tumor lysosomes while being nonfluorescent at extralysosomal setting are appealing tools for low-background tumor imaging. In this context, we set to examine the efficacy of a panel of lysosome-activatable glycan-presenting micelles to illuminate tumors in mice models (Fig. 1).

### Rhodamine-sultam for imaging of lysosomal acidity

Albeit widely used for bioimaging owing to their distinguished photophysical properties such as intensive fluorescence and bioorthogonal fluorescence spectra, rhodamines are pH insensitive. As such, nonfluorescent rhodamine-(deoxy)lactams featuring intra-molecular (deoxy)lactams have been developed for lysosome imaging in live cells where the acidic pH of the lysosomal lumen triggered fluorogenic opening of the spiro-(deoxy)lactams to give fluorescent rhodamine species (Fig. 2A).<sup>[13]</sup> However, rhodamine-lactams typically exhibit low levels of fluorescence emission at lysosomal pH whereas the use of rhodamine-deoxylactam, albeit sensitive to acidic pH, is compromised by its cross-reactivity to biological aldehydes.<sup>[14]</sup>

Sulfonamide is significantly more acidic (pKa~10) than amide (pKa~20-23). On the basis that sulfonamide is a better leaving group than the amide moiety, rhodamine-sultam (RST) is anticipated to be more vulnerable to the opening of intramolecular sultam as compared to rhodamine-lactams (Fig. 2B) and thus displays enhanced pH sensitivity. RST was prepared from coupling of sulforhodamine with ethylenediamine to give rhodamine-sulfonamide which spontaneously self-rearranges to yield the nonfluorescent RST (ESI†, Scheme. S1). Analysis of RST fluorescence emission in buffers of various pH shows that RST is 8-10 folds brighter than *N*-(rhodamine B)-lactam-ethylenediamine (RLT), the structural analog of RST, in the range of pH 4.0-6.5 which fully matches the lysosomal pH window (pH 6.5-4.0) (Fig. 2C). The UV-vis absorption spectrum and fluorescence spectra of RST in acidic media are almost identical to that of sulfo-rhodamine (ESI†, Fig. S1-S3), validating proton mediated isomerization of RST into the highly fluorescent rhodamine-sulfoamide as proposed in Fig. 2B.

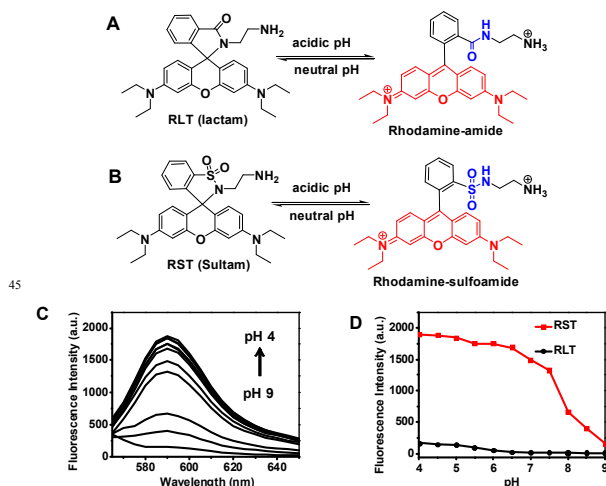


**Fig. 2** Acidic pH mediated fluorogenic opening of the sultam of RST and the lactam of RLT. RLT (A) and RST (B) were

respectively spiked into sodium-phosphate buffer (100 mM) of various pH values to a concentration of 1  $\mu$ M. The fluorescence emission of the resultant solutions was recorded using  $\lambda_{ex}$ @560 nm. (C) pH dependent fluorescence emission of RST; (D) pH profiles of RST (in red) and RLT (in dark) were plotted by fluorescence emission intensities@590 nm over buffer pH.

With the superior pH sensitivity, RST was evaluated for its capability to fluoresce in lysosomes. Raw 264.7 macrophages and human hepatocellular carcinoma QGY-7701 cells were respectively co-stained with RST and LysoTracker Green DND-26 (referred to as LysoTracker green). Confocal microscopy analysis shows that strong rhodamine fluorescence were clearly present within cells and colocalizes with LysoTracker green which is a lysosome specific marker (Fig. 3). The colocalization validates that RST becomes fluorescent within lysosomes. Next, Raw 264.7 cells and QGY-7701 cells pretreated with Bafilomycin A1 (BFA) were co-stained with RST and LysoTracker green. BFA inhibits the proton pumping activity of ATP-H1 pump and thus effectively alkalinizes the lysosomal pH.<sup>[15]</sup> It is shown that the intralysosomal fluorescence of RST largely disappeared in BFA-treated cells (Fig. 4), proving that RST is activated by lysosomal acidity to give fluorescent rhodamine-sulfonamide.

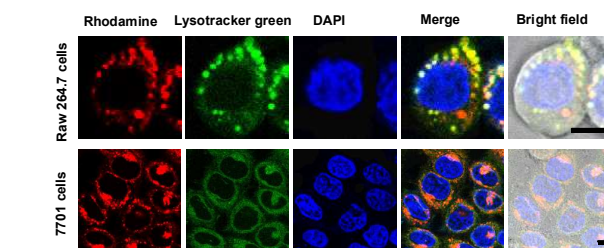


**Fig. 3** Selective staining of lysosomes with RST. Raw 264.7 cells and QGY-7701 cells prestained with DAPI (1  $\mu$ M) were respectively cultured in DMEM containing RST (1  $\mu$ M) for 30 min, and then stained with LysoTracker green (1  $\mu$ M) for 20 min. The nuclei stained with DAPI were shown in blue. Merging of RST fluorescence (shown in red) and that of LysoTracker green (in green) revealed colocalization, indicated by the yellow areas. Bars, 5  $\mu$ m.

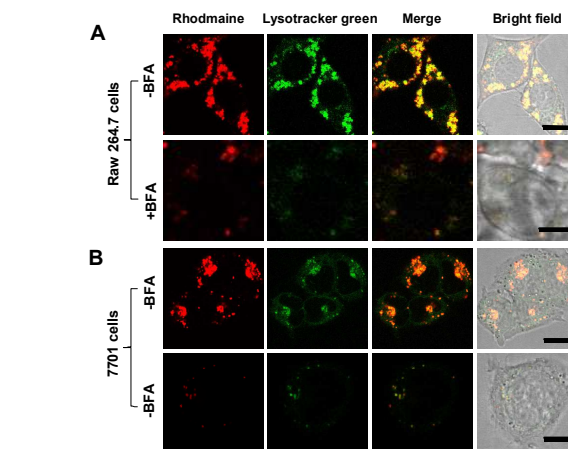


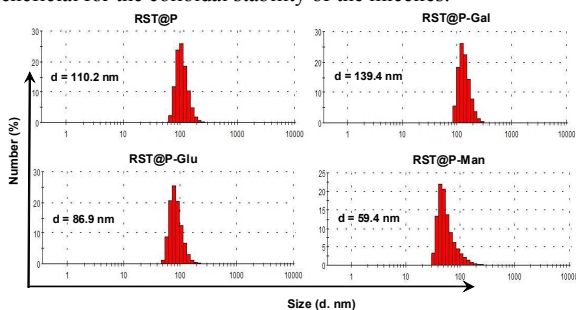
**Fig. 4** Lysosomal pH triggered fluorescence activation of RST. Raw 264.7 cells (A) and QGY-7701 cells (B) precultured in the absence or presence of BFA (50 nM) were first cultured in DMEM with RST (1  $\mu$ M) for 30 min and then stained with LysoTracker green (1  $\mu$ M) in DMEM for 20 min. The cells were visualized by confocal fluorescence microscopy. Overlay of RST

signal (in red) with LysoTracker green (in green) revealed colocalization, indicated by the yellow areas. Bars, 5  $\mu\text{m}$ .

### Construction and characterization of pH responsive micelles

Poly[styrene-*alter*-(maleic acid)] is biocompatible as its conjugate with neocarzinostatin has been marketed in Japan for treatment of primary hepatoma and secondary liver tumor.<sup>[16]</sup> We have previously shown that polyanionic poly[styrene-*alter*-(maleic acid)] derivatives are potent microbicides against HIV-1 infection<sup>[17]</sup> and exhibit low levels of nonspecific binding to mammalian cells owing to Coulombic repulsion with the negatively charged host cell surfaces.<sup>[18]</sup> Given these advantageous biomedical properties, poly[styrene-*alt*-(maleic acid)] was used as the carrier of RST and targeting glycans for fluorescence guided tumor detection.

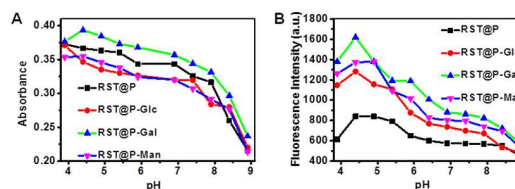
Poly[styrene-*alter*-(maleic anhydride)]<sub>40</sub> was partially amidated with RST and then respectively amidated with D-galactosamine (Gal), D-mannosamine (Man), D-glucosamine (Glu) in dimethylformamide (ESI<sup>†</sup>). The resultant solutions were treated with an aqueous solution of sodium carbonate to hydrolyze unreacted anhydride moieties, extensively dialyzed in distilled water, and then sonicated to afford poly[styrene-*alter*-(maleic acid-RST)] decorated with Man, Gal, or Glu, which are correspondingly designated as RST@P-Man, RST@P-Gal, and RST@P-Glu. In parallel, poly[styrene-*alter*-(maleic acid-RST)] was prepared and used as the glycan-free control (designated as RST@P). Dynamic light scattering analysis shows that the hydrodynamic diameters are 110.2 nm, 86.9 nm, 139.4 nm and 59.4 nm for RST@P, RST@P-Glu, RST@P-Gal, and RST@P-Man (Fig. 5), confirming that the as-prepared polymers self-assembled into nanoscaled micelles upon sonication in aqueous solutions. Zeta potentials of these micelles are in the range of -40 mv to -50 mv (ESI<sup>†</sup>, Fig. S4), which is consistent with the anionic nature of the micelles. The dense surface charges are beneficial for the colloidal stability of the micelles.



**Fig. 5** Diameter sizes of the nanoscaled micelles as measured by dynamic light scattering.

The micelles were respectively spiked into buffers of various pH (4-9) to probe their pH responsiveness. Analysis of the solutions by UV-vis spectroscopy showed that these RST-appended micelles display strong absorbance peaked at 560 nm under acidic pH (ESI<sup>†</sup>, Fig. S1), suggesting the formation of deep colored rhodamine-sulfoamide. The micelles exhibit fluorescence emission which is centered at 590 nm and intensifies as the buffer pH decreases (ESI<sup>†</sup>, Fig. S2). The levels of RST conjugated in these micelles are similar as determined by their UV-vis absorbance at acidic pH (Fig. 6A; ESI<sup>†</sup>, Fig. S5). In contrast, the glyco-micelles are more emissive than RST@P under acidic conditions (Fig. 6B), suggesting the beneficial impacts of the glycan moieties on fluorescence emission of conjugated RST. RST displays 10-fold fluorescence enhancement in pH 4.5 over pH 9.0 whereas RST@P-Gal exhibits 4-fold enhancement (Fig.

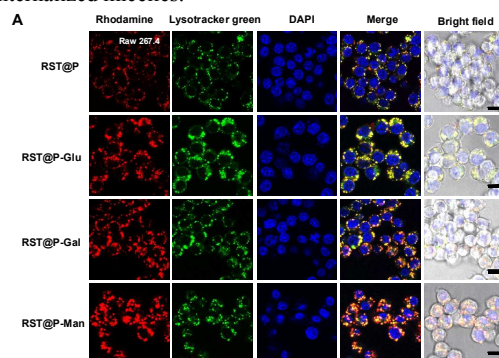
6B). The dampened fluorescence emission is likely owing to the interference of the polymeric carrier on fluorescence properties of pendent RST moieties under the assay conditions. Collectively, these titrations confirm that RST within micelles is poised to proton triggered fluorogenic opening of the sultam at acidic settings.



**Fig. 6** pH profiles of the micelles. The micelles were respectively spiked into sodium phosphate buffer (100 mM) of various pH (3.9-8.9) to a final concentration of 50  $\mu\text{g ml}^{-1}$  (A) or 10  $\mu\text{g ml}^{-1}$  (B). The solutions were analyzed by UV-vis spectrometry and the titration profiles were plotted using the absorbance at 560 nm (A) or the fluorescence emission (B) of the solutions over buffer pH ( $\lambda_{em}$ @590 nm;  $\lambda_{ex}$ @ 560 nm).

### Lysosomal acidity mediated fluorescence activation of the micelles

Lysosomes are the major acidic compartments within cells and the lysosomal pH is critical for a wealth of biological activities such as autophagy, endocytosis and cancer metastasis. Optical probes that could be selectively activated in lysosome are powerful tools for low-background cancer imaging.<sup>[3c, 4a]</sup> To probe the feasibility of lysosome mediated fluorescence activation, QGY-7701 cells and Raw 264.7 cells were respectively cultured with each of the micelles in medium supplemented with LysoTracker green. As shown in Fig. 7, rhodamine fluorescence is clearly present within micelle-treated cells where it colocalizes with LysoTracker green, proving that these micelles become fluorescent upon internalization into lysosomes. To ascertain the correlation of the intralysosomal fluorescence with lysosomal pH, we acquired the signals of the micelles in cells pretreated with BFA. The intracellular fluorescence largely vanished in BFA-treated cells (Fig. 8), confirming lysosomal acidity mediated fluorescence activation of the internalized micelles.



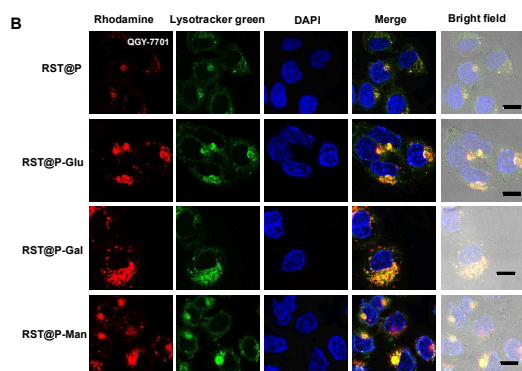


**Fig. 7** Illumination of lysosomes with the micelles. Raw 264.7 cells (A) and QGY-7701 cells (B) prestained with DAPI (1  $\mu\text{M}$ ) were respectively cultured for 30 min in DMEM supplemented with the indicated micelles (10  $\mu\text{g ml}^{-1}$ ), and then stained with Lysotracker green (1  $\mu\text{M}$ ) in DMEM for 20 min. Merging of the intracellular RST fluorescence shown in red and that of Lysotracker green shown in green demonstrates colocalization where yellow was observed. Bars, 10  $\mu\text{m}$ .

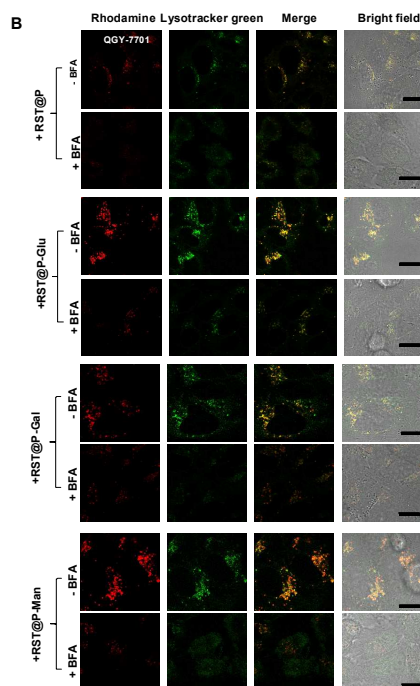
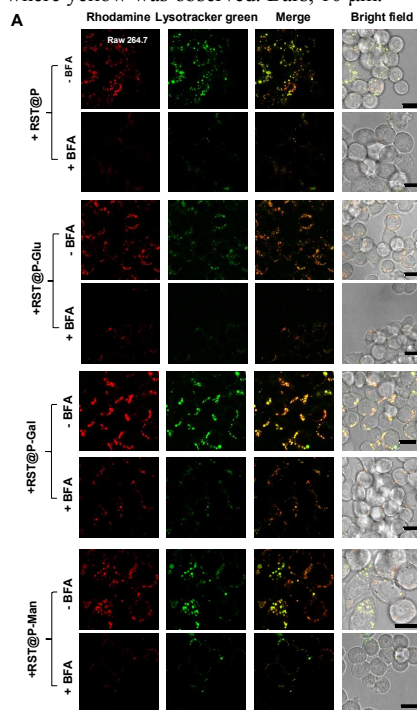


**Fig. 8** Lysosomal acidity mediated fluorescence activation of the micelles. Raw 264.7 cells (A) and QGY-7701 cells (B) pretreated with or without BFA were respectively treated with RST@P (10  $\mu\text{g ml}^{-1}$ ), RST@P-Glu (10  $\mu\text{g ml}^{-1}$ ), RST@P-Gal (1  $\mu\text{g ml}^{-1}$ ) or RST@P-Man (1  $\mu\text{g ml}^{-1}$ ) in DMEM for 30 min and then stained with Lysotracker green (1  $\mu\text{M}$ ) in DMEM for 20 min. The intracellular fluorescence of the micelles within cells was probed by confocal fluorescence microscopy. Merging of RST fluorescence shown in red and that of Lysotracker green shown in green demonstrate colocalization, indicated by the yellow areas. Bars, 10  $\mu\text{m}$ .

#### Lectin-mediated cellular uptake of the glyco-micelles

Lectins are abundantly expressed on cancer cells and the elevated levels of cell surface lectins are often associated with tumor clones with higher metastatic potentials.<sup>[19]</sup> Despite a few examples, *e.g.* galactose receptors identified on certain cancers,<sup>[20]</sup> information are lacking on the identity and density of functional lectins on various cancers. In addition, cancer cells express higher levels of glucose transporters than normal cells,<sup>[21]</sup> which underlies the use of glucose derivatives for imaging and treatment of cancers.<sup>[22]</sup> Given the heterogeneity of cell types in tumor foci, the micelles with multivalent monosaccharides of Gal, Man or Glu are directly screened for their efficacy to target tumors *in vivo* by tumoral lectins or glucose transporters.

As a proof of concept, Raw 264.7 cells and QGY-7701 cells were treated with the micelles to probe the influence of glycans on the cellular uptake of these micelles. No obvious fluorescence was identified in cells or culture medium right after addition of these micelles which is consistent with the nonfluorescent nature of the micelles at extracellular conditions. Flow cytometry analysis of the cells at 60 min post-incubation showed that RST@P-Man and RST@P-Gal were effectively internalized into both cell lines as determined by the mean channel fluorescence (MF) which is an indicator of the intracellular fluorescence intensity. RST@P-Glu entered cells with efficiency 50% that of RST@P-Man (Fig. 9) whereas the glycan-free RST@P exhibits low levels of cell uptake with MF values roughly 10-20% that of RST@P-Man or RST@P-Gal. Although the lectins targeted by these distinct glyco-micelles remains obscure at this stage, *e. g.* in

the cross-reactivity of Raw 264.7 cells to RST@P-Gal, the preferred cellular internalization of glyco-micelles over RST@P clearly supports the critical roles of glycans on the active uptake of the micelles by lectin-expressing mammalian cells.

Besides high-efficiency cellular accumulation, retention of the internalized imaging probes within lysosomes is another critical factor for practical tumor detection. QGY-7701 cells and Raw 264.7 cells pre-cultured with RST or each of the micelles were incubated in micelle-free culture medium. Cells were visualized by fluorescence microscopy to probe the amounts of micelles remained in lysosomes over time. It was shown that RST fluorescence within these cell populations remain largely unaffected up to 48 h (Fig. S7, S8, ESI<sup>†</sup>), suggesting superior lysosomal retention of RST and the RST-functionalized micelles.

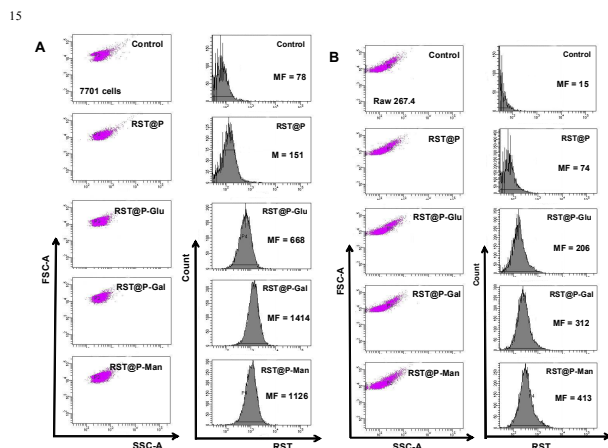


**Fig. 9** Flow cytometric analysis on differential cellular uptake of the micelles. QGY-7701 cells (A) and Raw 264.7 cells (B) were respectively cultured in DMEM spiked with or without the micelles ( $10 \mu\text{g ml}^{-1}$ ) for 60 min. The cells were washed with PBS and then analyzed by flow cytometry. The cell populations were gated under identical conditions and the intracellular fluorescence ( $\lambda_{em}@PE$  channel) was collected using  $\lambda_{ex}@488$  nm. The mean channel fluorescence (MF) values indicating the intracellular fluorescence intensity were measured and included.

#### Illumination of subcutaneous tumors with RST@P-Man and RST@P-Gal

On the basis of glycan-facilitated cellular endocytosis and lysosomes, we accessed whether these probes could target subcutaneous tumors in mice. H22 hepatocellular carcinoma cells were injected subcutaneously into the flank of ICR mice. Within 5-10 days after inoculation, the micelles were respectively injected into the bloodstreams of tumor-bearing ICR mice *via* tail vein. The mice were sacrificed 17 h post-injection and the biodistribution was assessed by measuring fluorescence emission in the dissected organs.

To our delight, the most intense signals are observed in tumors of mice treated RST@P-Gal or RST@P-Man, and surprisingly, no obvious uptake of RST@P-Glu is seen in the tumor (Fig. 10). Consistent with the previous report,<sup>[23]</sup> accumulation of RST@M was observed in the excised tumor (Fig. 10). The lack of fluorescence in the organs and the tumor from PBS-treated mice (Fig. 10) validates that the observed tumor-associated fluorescence originates from internalized micelles in mice. The preferred tumoral uptake of RST@P over RST@P-Glu reveals the limitations to predict *in vivo* performance of probes on the basis of their *in vitro* properties, *e.g.* elevated cellular accumulation of RST@P-Glu over RST@P (Fig. 9). The high

tumor to background fluorescence ratios displayed by RST@P-Gal or RST@P-Man (Fig. 10B) validate the feasibility to illuminate tumors *in vivo* with responsive glyco-micelles which undergo fluorescence activation upon tumor lectin-mediated endocytosis into the lysosomes.

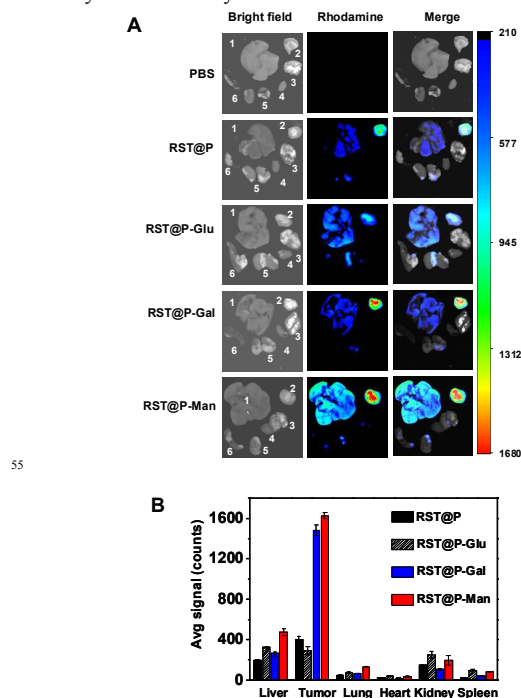


**Fig. 10** High-efficiency illumination of subcutaneous tumors with RST@P-Gal and RST@P-Man. ICR mice with subcutaneous tumors were intravenously injected with each of the micelles ( $10 \text{ mg kg}^{-1}$ ) or PBS via tail vein and then sacrificed 17 h post-injection. The tumors and representative organs were dissected and imaged by *ex vivo* fluorescence analysis (A). The bar graph shows the tissue distributions of RST fluorescence (B). The organs were shown in the following sequence: liver (1), tumor (2), lung (3) heart (4), kidney (5) and spleen (6).

To probe temporal retention of the micelles in tumors, a cohort of mice with subcutaneous tumors were intravenously administered with these micelles and then sacrificed at 4, 10, 17 or 39 h following injection. RST fluorescence in the tumors and other organs was determined *ex vivo*. As shown in Fig. S9 (ESI<sup>†</sup>), high-efficiency accumulation of RST@P-Man and RST@P-Gal were observed in tumors at 17 h post-injection, which decreased dramatically to background levels by 39 h post-injection. Concurrently, the liver-associated fluorescence in mice treated with both glyco-micelles significantly lowered (Fig. S9, ESI<sup>†</sup>), suggesting liver is the major excretion organ of these polymeric agents.

#### High resolution imaging of liver tumor foci with RST@P-Gal

Liver cancer, constituted mostly by hepatocellular carcinoma, is one of the most common and lethal malignancies with over 600,000 new cases diagnosed annually and roughly equal number of deaths.<sup>[24]</sup> Albeit offering limited chances to cure, cytoreductive surgery corroborated chemotherapy remains the major modality for treatment of liver cancer. Hence, approaches that could assist complete surgical removal of cancer cells will in principle lead to cancer cure. To ascertain whether the glyco-micelles could be used to discern tumor foci in liver, ICR mice with H22 hepatocellular carcinoma in the liver were

intravenously administered with the micelles. At 15 h after injection, the liver and other healthy organs were excised and probed *ex vivo*. No fluorescence is observed in tumors excised from mice treated with RST@P-Man, RST@P-Glu or RST@P (Fig. 11). In sharp contrast, intensive fluorescence is observed in disseminated tumor foci with diameters in the ranges of 0.1-5 mm in the liver from RST@P-Gal-treated mice (Fig. 11B).

Symptoms of human hepatocellular carcinoma often occur till the tumor reaches 4-8 cm in diameter.<sup>[25]</sup> As incomplete surgical removal of tumor foci often leads to treatment failure, a minimum of 1-cm clearance, defined as minimal residual disease, was aimed by most surgeons during resection of many cancers.<sup>[26]</sup> As demonstrated in Fig. 11, the sizes of tumor foci unambiguously differentiated by RST@P-Gal (0.1-5 mm) are significantly below current limit of minimal residual cancer (tumor deposit < 1cm). Given the facts that hepatocytes efficiently capture nanoscaled materials or galactose-presenting proteins,<sup>[27]</sup> the capability of RST@P-Gal to illuminate tumor foci at sub-mm levels and the stringent selectivity for tumor over neighboring liver tissue highlight its clinical potentials to improve surgical resection of tumor foci that are otherwise elusive to visual inspection during surgery. Galactose-containing proteins have been documented to bind a number of different tumors, suggesting the presence of galactose receptors in these tumors.<sup>[20a]</sup> In addition, nanomaterials have been widely used for tumors imaging by enhanced permeability and retention (EPR) effects.<sup>[28]</sup> The tumor-specific accumulation of RST@P-Gal is likely due to a combination of passive targeting via EPR effects and subsequent active targeting by tumor surface lectin mediated absorption of local micelles.

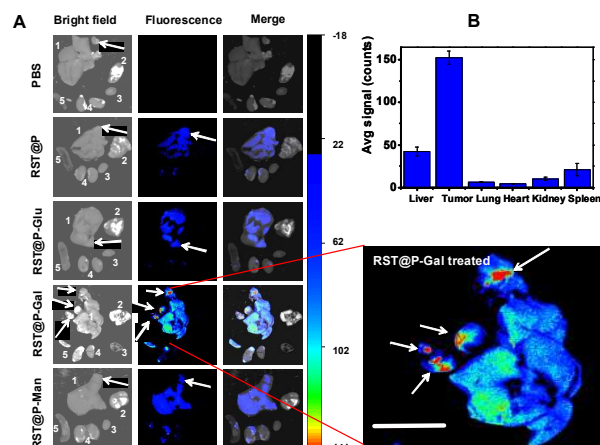


**Fig. 11** High resolution illumination of tumor foci (white arrows) in liver with RST@P-Gal. ICR mice with liver tumors were intravenously injected with PBS or each of the micelles (10 mg kg<sup>-1</sup>) via tail vein, sacrificed 15 h post-injection. The representative organs were excised and visualized *ex vivo* by fluorescence analysis (A). Enlarged fluorescence image of the liver from RST@P-Gal treated mice was shown for clarity. Bar: 1 cm. (B) The bar graph shows the fluorescence intensity of RST@P-Gal in tumor foci vs surrounding liver tissue and other organs. The organs are arrayed in the following sequence: liver (1), lung (2), heart (3) kidney (4) and spleen (5).

### Cytotoxicity of the micelles

The cytotoxicity of the micelles was evaluated in QGY-7701 cells and Raw 264.7 cells by Trypan Blue exclusion test. No detrimental effects on cell viability were observed at doses up to 100  $\mu\text{g ml}^{-1}$  after incubation up to 48 h (Fig. 12), suggesting that these polymers are of low cell toxicity. To investigate the

systemic toxicity, RST@P-Gal was respectively injected by tail vein at doses up to 100 mg kg<sup>-1</sup> in healthy mice, which is 10 times higher than the amount employed for tumor imaging. The mice were regularly monitored for adverse effects following injections. No signs of toxicity, pain or fatigue were observed on the mice receiving the micelles up to 7 days following injection. *Ex vivo* analysis revealed low levels of fluorescence in the organs excised from the mice (ESI†, Fig. S10), suggesting that these micelles might have been cleared from the body. The biocompatibility of poly[styrene-*alter*-(maleic acid)] has been demonstrated by its conjugate marketed for treatment of liver tumors.<sup>[16]</sup> Consistently, these data indicate that these polymeric micelles are of low cellular and systemic toxicity.

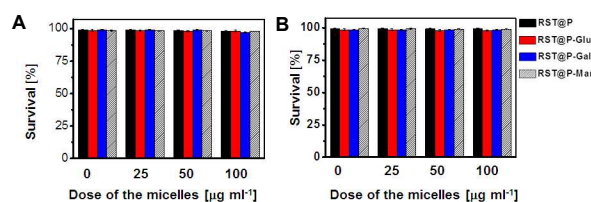


**Fig. 12** Cytotoxicity of the micelles. QGY-7701 cells (A) and Raw 264.7 cells (B) were culture for 24 h in DMEM medium supplemented with various amounts of the micelles as indicated (0, 25, 50, 100  $\mu\text{g ml}^{-1}$ ). The cell number and cell viability were determined by trypan blue exclusion.

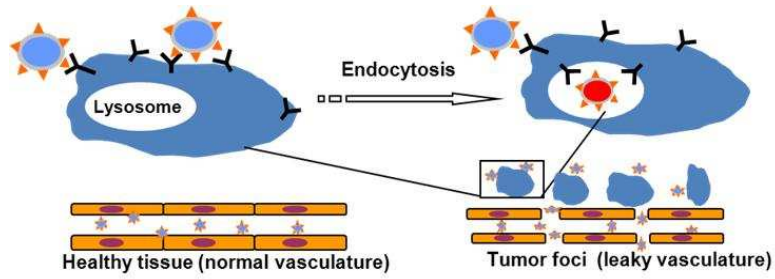
### Conclusions

We demonstrate the use of acid-responsive glyco-micelles for targeted tumor imaging in mice models. High-performance *in vivo* illumination of disseminated liver tumors and subcutaneous tumors was achieved with RST@P-Gal featuring lysosome activatable rhodamine-sultam (RST). RST is nonfluorescent extracellularly and is poised to lysosomal pH mediated fluorescence activation, allowing optical tracking of glyco-micelles within viable cancer cells. With the high resolution to discern tumor foci, intense intratumoral fluorescence and low background signals, RST@P-Gal is of clinical utility for fluorescence-guided surgical ablation of liver tumors. As different tumors often display distinct lectins, this system is readily adaptable to illuminate different tumors by incorporation of appropriate glycans on the corona. The lectin-targeted multifunctional system offers an effective and facile approach for *in vivo* optical tracking of tumors and thus would be of broad potentials for cancer diagnosis and surgery.

### Notes and references

<sup>a</sup>Department of Chemical Biology, College of Chemistry and Chemical Engineering, the Key Laboratory for Chemical Biology of Fujian Province, The MOE Key Laboratory of Spectrochemical Analysis & Instrumentation, and Innovation Center for Cell Biology, Xiamen University; <sup>b</sup>State key Laboratory of Cellular Stress Biology, Innovation Center for Cell Biology, School of Life Sciences, Xiamen University, Xiamen, 361005, China; Tel: 86-0592-2181728; E-mail: [shoufa@xmu.edu.cn](mailto:shoufa@xmu.edu.cn)  
<sup>95</sup> Acknowledgments: Dr. S. Han was supported by grants from 973 program 2013CB93390, NSF China (21272196, 21072162), PCSIRT, and the Fundamental Research Funds for the Central Universities (2011121020); Dr. J. Han was supported by grants from NSF China (30830092, 30921005, 91029304, 81061160512).  
<sup>100</sup> † Electronic Supplementary Information (ESI) available on experimental procedures; synthesis and characterization of RST and glyco-micelles; stability of RST@P-Gal in buffers of various pH values, UV-vis titration of RST levels in RST@P-Gal; additional data for imaging of micelle-cell interactions by confocal fluorescence microscopy, and systemic toxicity of the micelles in mice. See DOI: 10.1039/b000000x/

- 1 Q. T. Nguyen, R. Y. Tsién, *Nat. Rev. Cancer* 2013, **13**, 653.
- 2 G. M. van Dam, G. Themelis, L. M. Crane, N. J. Harlaar, R. G. Pleijhuis, W. Kelder, A. Sarantopoulos, J. S. de Jong, H. J. Arts, A. G. van der Zee, J. Bart, P. S. Low, V. Ntziachristos, *Nat. Med.*, 2011, **17**, 1315.
- 5 (a) Y. Urano, M. Sakabe, N. Kosaka, M. Ogawa, M. Mitsunaga, D. Asanuma, M. Kamiya, M. R. Young, T. Nagano, P. L. Choyke, H. Kobayashi, *Sci. Transl. Med.* 2011, **3**, 110ra119; (b) Q. T. Nguyen, E. S. Olson, T. A. Aguilera, T. Jiang, M. Scadeng, L. G. Ellies, R. Y. Tsién, *Proc. Natl. Acad. Sci.*, 2010, **107**, 4317; (c) Y. Urano, D. Asanuma, Y. Hama, Y. Koyama, T. Barrett, M. Kamiya, T. Nagano, T. Watanabe, A. Hasegawa, P. L. Choyke, H. Kobayashi, *Nat. Med.*, 2009, **15**, 104.
- 4 (a) H. Kobayashi, P. L. Choyke, *Acc. Chem. Res.*, 2011, **44**, 83; (b) H. Kobayashi, M. Ogawa, R. Alford, P. L. Choyke, Y. Urano, *Chem. Rev.*, 2010, **110**, 2620; (c) K. Sokolov, D. Nida, M. Descour, A. Lacy, M. Levy, B. Hall, S. Dharmawardhane, A. Ellington, B. Korgel, R. Richards-Kortum, *Adv. Cancer Res.*, 2007, **96**, 299; (d) U. Mahmood, R. Weissleder, *Mol. Cancer Ther.*, 2003, **2**, 489; (e) S. Kumar, R. Richards-Kortum, *Nanomedicine*, 2006, **1**, 23; (f) K. Sokolov, J. Aaron, B. Hsu, D. Nida, A. Gillenwater, M. Follen, C. MacAulay, K. Adler-Storthz, B. Korgel, M. Descour, R. Pasqualini, W. Arap, W. Lam, R. Richards-Kortum, *Technol. Cancer Res. Treat.*, 2003, **2**, 491; (g) H. Lee, W. Akers, K. Bhushan, S. Bloch, G. Sudlow, R. Tang, S. Achilefu, *Bioconjug. Chem.*, 2011, **22**, 777.
- 25 C. F. Brewer, M. C. Miceli, L. G. Baum, *Curr. Opin. Struct. Biol.*, 2002, **12**, 616.
- 6 N. Yamazaki, S. Kojima, N. V. Bovin, S. Andre, S. Gabius, H. J. Gabius, *Adv. Drug Deliv. Rev.*, 2000, **43**, 225.
- 30 7 B. E. Collins, J. C. Paulson, *Curr. Opin. Chem. Biol.*, 2004, **8**, 617-625.
- 8 P. D. Stahl, *Curr. Opin. Immunol.*, 1992, **4**, 49.
- 9 (a) C. J. Van Den Hamer, A. G. Morell, I. H. Scheinberg, J. Hickman, G. Ashwell, *J. Biol. Chem.*, 1970, **245**, 4397; (b) G. Ashwell, J. Harford, *Annu. Rev. Biochem.*, 1982, **51**, 531.
- 35 10 (a) C. H. Wu, G. Y. Wu, *Adv. Drug Deliv. Rev.*, 1998, **29**, 243; (b) R. T. Lee, P. Lin, Y. C. Lee, *Biochemistry*, 1984, **23**, 4255; (c) S. Sonoke, T. Ueda, K. Fujiwara, K. Kuwabara, J. Yano, *Biol. Pharm. Bull.*, 2011, **34**, 1338; (d) P. Ma, S. Liu, Y. Huang, X. Chen, L. Zhang, X. Jing, *Biomaterials*, 2010, **31**, 2646; (e) C. Managit, S. Kawakami, F. Yamashita, M. Hashida, *Int. J. Pharm.*, 2005, **301**, 255; (f) M. H. Lee, J. H. Han, P. S. Kwon, S. Bhuniya, J. Y. Kim, J. L. Sessler, C. Kang, J. S. Kim, *J. Am. Chem. Soc.*, 2012, **134**, 1316; (g) M. Hashida, K. Akamatsu, M. Nishikawa, F. Yamashita, Y. Takakura, *J. Control Release*, 1999, **62**, 253; (h) B. Guo, Y. Cheng, N. Li, X. Li, M. Jin, T. Li, J. Li, *J. Drug Target*, 2012; 257; (i) R. Kikkeri, B. Lepenies, A. Adibekian, P. Laurino, P. H. Seeberger, *J. Am. Chem. Soc.*, 2009, **131**, 2110.
- 11 (a) L. Cui, J. A. Cohen, K. E. Broaders, T. T. Beaudette, J. M. Frechet, *Bioconjug. Chem.*, 2011, **22**, 949; (b) H. L. Jiang, M. L. Kang, J. S. Quan, S. G. Kang, T. Akaike, H. S. Yoo, C. S. Cho, *Biomaterials*, 2008, **29**, 1931; (c) K. Movahedi, S. Schoonooghe, D. Laoui, I. Houbracken, W. Waelput, K. Breckpot, L. Bouwens, T. Lahoutte, P. De Baetselier, G. Raes, N. Devoogdt, J. A. Van Ginderachter, *Cancer Res.*, 2012, **72**, 4165; (d) L. M. Artner, L. Merkel, N. Bohlke, F. Beceren-Braun, C. Weise, J. Dermedde, N. Budisa, C. P. Hackenberger, *Chem. Commun.*, 2012, **48**, 522; (e) P. Chenevier, C. Grandjean, E. Loing, F. Malingue, G. Angyalosi, H. Gras-Masse, D. Roux, O. Melnyk, L. Bourel-Bonnet, *Chem. Commun.*, 2002, **20**, 2446; (f) F. Orsini, P. Villa, S. Parrella, R. Zangari, E. R. Zanier, R. Gesuete, M. Stravalaci, S. Fumagalli, R. Ottria, J. J. Reina, A. Paladini, E. Micotti, R. Ribeiro-Viana, J. Rojo, V. I. Pavlov, G. L. Stahl, A. Bernardi, M. Gobbi, M. G. De Simoni, *Circulation*, 2012, **126**, 1484; (g) U. Wattendorf, G. Coullerez, J. Voros, M. Textor, H. P. Merkle, *Langmuir*, 2008, **24**, 11790; (h) R. Su, L. Li, X. Chen, J. Han, S. Han, *Org. Biomol. Chem.*, 2009, **7**, 2040.
- 12 (a) M. H. El-Dakdouki, D. C. Zhu, K. El-Boubbou, M. Kamat, J. Chen, W. Li, X. Huang, *Biomacromolecules*, 2012, **13**, 1144; (b) N. Kawasaki, J. L. Vela, C. M. Nycholat, C. Rademacher, A. Khurana, N. van Rooijen, P. R. Crocker, M. Kronenberg, J. C. Paulson, *Proc. Natl. Acad. Sci.*, 2013, **110**, 7826.
- 13 (a) Q. A. Best, C. Liu, P. D. van Hoveln, M. E. McCarroll, C. N. Scott, *J. Org. Chem.*, 2013, **78**, 10134; (b) Q. A. Best, R. Xu, M. E. McCarroll, L. Wang, D. J. Dyer, *Org Lett* 2010, **12**, 3219; cZ. Li, Y. Song, Y. Yang, L. Yang, X. Huang, J. Han, S. Han, *Chem. Sci.*, 2012, **3**, 2491; (d) S. Wu, Z. Li, J. Han, S. Han, *Chem. Commun.*, 2011, **47**, 11276; (e) T. Hasegawa, Y. Kondo, Y. Koizumi, T. Sugiyama, A. Takeda, S. Ito, F. Hamada, *Bioorg. Med. Chem.*, 2009, **17**, 6015; (f) Z. Li, S. Wu, J. Han, S. Han, *Analyst*, 2011, **136**, 3698; (g) H. Zhu, J. Fan, Q. Xu, H. Li, J. Wang, P. Gao, X. Peng, *Chem. Commun.*, 2012, **48**, 11766; (h) W. Zhang, B. Tang, X. Liu, Y. Liu, K. Xu, J. Ma, L. Tong, G. Yang, *Analyst*, 2009, **134**, 367.
- 14 Z. Li, Z. Xue, Z. Wu, J. Han, S. Han, *Org. Biomol. Chem.*, 2011, **9**, 7652.
- 85 15 T. Yoshimori, A. Yamamoto, Y. Moriyama, M. Futai, Y. Tashiro, *J. Biol. Chem.*, 1991, **266**, 17707.
- 16 H. Maeda, *Adv. Drug Deliv. Rev.*, 2001, **46**, 169.
- 17 W. Fang, Y. Cai, X. Chen, R. Su, T. Chen, N. Xia, L. Li, Q. Yang, J. Han, S. Han, *Bioorg. Med. Chem. Lett.*, 2009, **19**, 1903.
- 90 18 L. Yang, S. Wu, B. Lin, T. Huang, X. Chen, X. Yan, S. Han, *J. Mater. Chem. B*, 2013, **1**, 6115.
- 19 R. Lotan, A. Raz, *Ann. N. Y. Acad. Sci.*, 1988, **551**, 385.
- 20 (a) Y. Hama, Y. Urano, Y. Koyama, P. L. Choyke, H. Kobayashi, *Biochem. Biophys. Res. Commun.*, 2006, **348**, 807; (b) A. Raz, R. Lotan, *Cancer Res.*, 1981, **41**, 3642.
- 95 21 (a) L. Szablewski, *Biochim. Biophys. Acta.*, 2013, **1835**, 164; (b) T. J. Wheeler, P. C. Hinkle, *Annu. Rev. Physiol.*, 1985, **47**, 503; (c) R. A. Medina, G. I. Owen, *Biol. Res.*, 2002, **35**, 9.
- 100 22 (a) M. M. Abouzieed, E. S. Crawford, H. A. Nabi, *J. Nucl. Med. Technol.*, 2005, **33**, 145; (b) Y. S. Lin, R. Tungpradit, S. Sinchaikul, F. M. An, D. Z. Liu, S. Phutrakul, S. T. Chen, *J. Med. Chem.*, 2008, **51**, 7428.
- 23 Z. Li, Y. Song, Y. Yang, L. Yang, X. Huang, J. Han, S. Han, *Chem. Sci.*, 2012, **3**, 2941.
- 105 24 (a) D. Y. Kim, K. H. Han, *Liver Cancer*, 2012, **1**, 2; (b) P. Ferenci, M. Fried, D. Labrecque, J. Bruix, M. Sherman, M. Omata, J. Heathcote, T. Piratsivuth, M. Kew, J. A. Otegbayo, S. S. Zheng, S. Sarin, S. S. Hamid, S. B. Modawi, W. Fleig, S. Fedail, A. Thomson, A. Khan, P. Malfertheiner, G. Lau, F. J. Carillo, J. Krabshuis, A. Le Mair, *J. Clin. Gastroenterol.*, 2010, **44**, 239; (c) M. Sherman, *Semin. Liver Dis.*, 2010, **30**, 3.
- 25 (a) M. Colombo, *J. Hepatol.*, 1992, **15**, 225; (b) F. Trevisani, M. C. Cantarini, J. R. Wands, M. Bernardi, *Carcinogenesis*, 2008, **29**, 1299.
- 115 26 (a) M. Partridge, S. R. Li, S. Pateromicelakis, R. Francis, E. Phillips, X. H. Huang, F. Testa-Selase, J. D. Langdon, *Clin. Cancer Res.*, 2000, **6**, 2718; (b) K. Pantel, T. J. Moss, *Cytotherapy*, 1999, **1**, 53.
- 120 27 (a) T. Kasuya, S. Kuroda, *Expert Opin. Drug Deliv.*, 2009, **6**, 39; (b) J. D. Perkins, *Liver Transpl.*, 2007, **13**, 167.
- 28 (a) H. Maeda, J. Wu, T. Sawa, Y. Matsumura, K. Hori, *J. Control Release*, 2000, **65**, 271; (b) V. Torchilin, *Adv. Drug Deliv. Rev.*, 2011, **63**, 131.
- 125



High-performance illumination of subcutaneous tumor and liver tumor foci at sub-millimeter levels was achieved with lectin-targeted glyco-micelles which become fluorescent upon internalization into tumor lysosomes.